ELSEVIER

Nuclear Physics B (Proc. Suppl.) 60B (1998) 105–116

NUCLEAR PHYSICS B
PROCEEDINGS
SUPPLEMENTS

Cosmic ray studies around the "knee" of the primary spectrum from EAS-TOP

G. Navarra[a] *

[a]Dipartimento di Fisica Generale dell'Università - INFN - CNR
Via P. Giuria 1, 10125 Torino, Italy

The experimental information on primary cosmic rays in the energy range $10^{14} - 10^{16}$ eV is discussed following the present data from the EAS-TOP array (Campo Imperatore, 2000 m a.s.l., INFN National Gran Sasso Laboratories).
The data on the "knee", as observed in the electromagnetic and muon components ($E_\mu \geq$ GeV) are presented. They are consistent both concerning the intensity and the primary energy of the break, and the slopes of the spectra below and above the steepening. From the e.m. size spectrum: the shape of the break, the dependence of its size on the atmospheric depth and the primary energy spectrum are derived.
The data on the sidereal anisotropy at $\bar{E}_o \approx 2. \cdot 10^{14}$ eV are discussed. The anisotropy is measured with good statistical accuracy: its amplitude is significantly smaller than expected from the diffusion models constructed at $10^9 - 10^{11}$ eV, showing that such models cannot be naively extrapolated to the 10^{14} eV energy range.

1. INTRODUCTION

The main feature of the cosmic ray data in the energy range $10^{14} - 10^{17}$ eV is represented by the break in the shower size (Ne) spectrum at $Ne \approx 10^6$ particles, first observed by the MSU group [1] and then by different experiments [2–9]. This has lead, as the most natural interpretation, to the hypothesis of a steepening of the primary cosmic ray spectrum at primary energy $E_o \approx (2 - 3) \cdot 10^{15}$ eV (the so called "knee"). Reasons for such steepening can be found either in propagation processes (decrease of containment in the galaxy with increasing particle energy, leading to a primary composition becoming reacher in heavy elements [10,11]), or in source effects, such as: energy limitations of the acceleration processes (upper limit to the maximum reachable energy as at the shock front in SNRs [12]) or nuclear fragmentation at the acceleration region (leading to lighter composition at higher energies [13]). Stimulating models incorporating in a single scenario the cosmic ray acceleration processes over the whole quoted energy range have recently been proposed [14] and have to be checked experimentally. Alternative interpretations of the break, as connected to a change in the hadronic interaction properties, have been proposed [15], also grounded on some inconsistencies in the Extensive Air Shower (EAS) data. Understanding the nature of the break requires accurate measurements of the different EAS components both to verify the main features of the hadronic physics, and to measure the variations with energy of the primary spectrum and composition (as interesting reviews on the subject see

*on behalf of the EAS-TOP collaboration: M. Aglietta[a,b], B. Alessandro[b], P. Antonioli[c], F. Arneodo[d,e], L. Bergamasco[b,f], M. Bertaina[b,f], A. Campos Fauth[g], C. Castagnoli[a,b], A. Castellina[a,b], A. Chiavassa[b,f], G. Cini Castagnoli[b,f], B. D'Ettorre Piazzoli[h], G. Di Sciascio[h], W. Fulgione[a,b], P. Galeotti[b,f], P.L. Ghia[a,b] M. Iacovacci[h], A. Lima de Godoi[g], G. Mannocchi[a,b], C. Melagrana[b,f], N. Mengotti Silva[g], C. Morello[a,b], G. Navarra[b,f], H. Nogima[g], L. Riccati[b], O. Saavedra[b,f], G.C. Trinchero[a,b], P. Vallania[a,b], S. Vernetto[a,b], C. Vigorito[b,f]. [a]Istituto di Cosmo-Geofisica del CNR, Corso Fiume 4, 10133 Torino, Italy [b]Istituto Nazionale di Fisica Nucleare, Via Pietro Giuria 1, 10125 Torino, Italy [c]Istituto Nazionale di Fisica Nucleare, Via Irnerio 46, 40126 Bologna, Italy [d]Dipartimento di Fisica dell' Università dell'Aquila, Via Vetoio, 67010 L'Aquila, Italy [e]INFN Laboratori Nazionali del Gran Sasso, S.S. 17 bis, 67010 Assergi (AQ), Italy [f]Dipartimento di Fisica Generale dell' Università, Via P. Giuria, 1, 10125 Torino, Italy [g]Instituto di Fisica, Universidade Estadual, Barao Geraldo, 13081 Campinas (SP), Brazil [h]Dipartimento di Scienze Fisiche dell' Università and INFN, Mostra D'Oltremare, 80125 Napoli, Italy.

0920-5632/98/$19.00 Elsevier Science B.V.
PII S0920-5632(97)00505-7

e.g. refs. [16,17], that contain full references.) Moreover, the internal consistency of the observations has to be checked, and indeed it has been questioned whether its lack could cast doubts on the existence itself of the break [17].

On another side the astrophysical interpretation of the knee, besides the knowledge of the composition variations, that can of course be of different origins, requires further experimental information. Among them, of main significance are the anisotropy data, that could discriminate propagation models, or at least help in checking the models themselves.

In this note we will discuss the general features of the break as observed in the electron and muon components by the EAS-TOP array at the Gran Sasso laboratories and the anisotropy data obtained at $\bar{E}_o \approx 2 \cdot 10^{14}$ eV, and their implications in connection with the interpretations of the knee in the primary spectrum.

2. THE ARRAY AND THE DATA TREATMENT

The EAS-TOP array [18] is located at Campo Imperatore (2000 m a.s.l., 810 g/cm^2 atmospheric depth, National Gran Sasso Laboratories). Its aims are to perform multi-informative and multi-component observations of Extensive Air Showers in the range between 10^{14} and 10^{16} eV, i.e. around the observed "knee". It includes detectors of the electromagnetic (e.m.), muon, hadron, atmospheric Cherenkov light components. Moreover it can run in coincidence with the muon detectors operating in the deep underground Gran Sasso laboratories (MACRO, LVD at muon energy threshold $E_\mu^{th} \approx 1.4$ TeV) (see figs. 1,2).

We are essentially interested here in the electromagnetic and muon detector data.

2.1. The e.m. component: detector, reconstruction and simulations

The e.m. detector [19,20] is made of 35 scintillator modules (10 m^2 each, 4 cm thick, divided into 16 individual units), organized in circles of radii r= 50-80 m, interconnected with each other, for trigger and data taking organization. The events used in the following discussion are characterized by at least 6-7 detectors fired (one located at the center and 5-6 on the quoted circle), and the maximum particle density recorded by a module internal to the edges of the array (for the measurement of the shower size spectrum, only events internal to the reduced area of fig. 1 are used). The EAS arrival direction is obtained through the times of flight among the different detectors, the accuracy being $\sigma_\alpha = 0.5^o$ for $Ne > 10^5$. The core location, the slope (s) of the lateral distribution function (*ldf*) and the shower size (N_e) are determined by means of a χ^2 fit in which the densities recorded by each module are compared with the theoretical NKG *ldf* [21,22] expression:

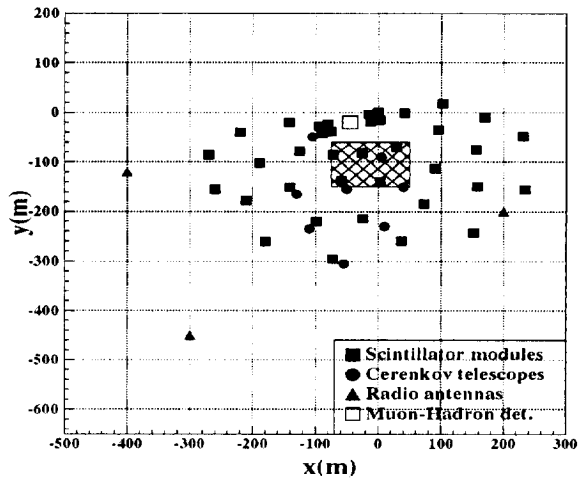

Figure 1. The EAS-TOP array. The shaded area shows the core location region used for the shower size spectrum measurement.

$$\rho(r) = \frac{C(s)Ne}{r_0^2}\left(\frac{r}{r_0}\right)^{s-2}\left(1+\frac{r}{r_0}\right)^{s-4.5} \quad m^{-2}(1)$$

with $r_0 = 100\ m$.

The validity of the NKG formula to describe the experimental data has been checked in every size interval, and it results to be accurate up to <10% in every range of core distances relevant to our measurements ($r < 200$ m).

The accuracy in the measurement of the size Ne has been obtained by analyzing showers simulated including all experimental dispersions: for $Ne > 10^5$ we obtain $\Delta Ne/Ne < 15\%$

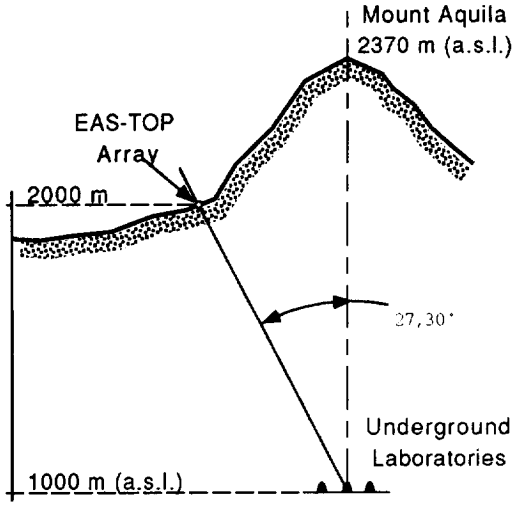

Figure 2. The EAS-TOP array location with respect to the underground Gran Sasso laboratories.

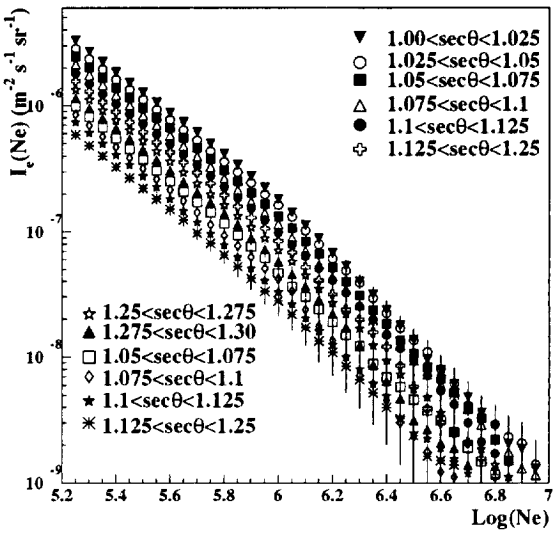

Figure 3. Integral size spectra measured at different zenith angles.

($\Delta Ne/Ne < 10\%$ for $Ne > 10^{5.2}$). The reconstruction procedures and accuracies are fully discussed in ref. [20].

The shower size expressed in units of *m.i.p.* (Ne^{mip}) is converted to total number of charged particles (Ne, defined as the number of charged particles with energy $E > 0$ at the depth of the detector following the Greisen formula [22]) by taking into account the transition effect in the scintillators. This has been studied by means of a simulation of the shower development in the atmosphere and in the detectors and their housing, based on the GEANT code [23]. We obtain that, up to 40°, the relation between Ne^{mip} and Ne is independent from the zenithal angle and is given by expression (a):

$$\frac{Ne^{mip}}{Ne} = 1.18 \qquad (2)$$

The full response of the detector to e.m. cascades has been verified by means of a test performed, with the same scintillators and electronics operating on the field, at a CERN positron beam up to e^+ energies $E_{e+} = 50$ GeV. A carbon target of thickness up to 15 r.l., increased by steps of 1.3 r.l. each, has been used. The calculated response, for age parameter $s > 0.6$, is verified within 3%.

The systematic distortions of the spectrum introduced by the experimental uncertainties have been studied by means of complete simulations. This results in a systematic correction to be applied to each bin content C (b): $\Delta C/C \approx 0.94(Ne/10^6)^{\Delta\gamma}$,with $\Delta\gamma = 0.08$ for $Ne < 10^6$ and $\Delta\gamma = 0.01$ for $Ne > 10^6$.

All comparisons with expectations are performed by using the Corsika code [24], with DPM model and Gheisha option for $E_h < 80$ GeV.

The resulting mean conversion from shower size to primary energy for vertical incidence can be expressed as in the following:

$$Ne = m(A)E_0^{n(A)} \qquad (3)$$

with

$$m(A) = 177.8A^{-0.52} \quad n(A) = 1.107A^{0.035}. \qquad (4)$$

Before converting from shower size to primary energy the further effect of fluctuations of the EAS development has to be taken into account

(c). Such fluctuations, as a function of primary energy, for primary protons, and following the Corsika code, are:

$$\frac{\sigma(Ne)}{Ne} = 0.44 - 0.15\frac{E_0(TeV)}{100} \qquad (5)$$

2.2. The muon detector

The muon detector [25] is composed of 9 active planes interleaved by 13 cm thick iron absorbers. The surface of the detector is 140 m^2 and its height 2.8 m. Each plane is made of two layers of streamer tubes for muon tracking and one layer of proportional tubes for hadron calorimetry. Every tube has 3 x 3 cm^2 section and 12 m length. The tracks X coordinates are obtained by the signals of the anode wires, the Y ones by the induced signals on strips (3 cm width) placed orthogonally to the wires. The muon energy threshold is $E_\mu \approx 1$ GeV for vertical incidence, the resolution (i.e. the difference between the numbers of visible and reconstructed muons with at least 6 wires and strips fired) is $\Delta N\mu^{det}/N\mu^{det} < 4.3\%$ up to $N_\mu^{det} = 30$, and, concerning the angles, $\Delta\theta_\mu \approx 0.6^o$.

3. THE E.M. DETECTOR DATA

3.1. The N_e spectrum and the all particle primary energy spectrum

The shower size spectrum is studied following the usual "constant intensity cut" technique [2] as shown in figs. 3,4.

The obtained EAS absorbtion length is $\Lambda = 220 \pm 6$ g cm^{-2}. Each individual shower size $Ne(\theta)$ recorded at zenith angle θ is therefore converted to vertical incidence ($Ne(0)$) with expression:

$$Ne(0) = Ne(\theta)e^{x_o(sec(\theta)-1)/\Lambda}. \qquad (6)$$

The spectra of fig. 3 are thus displayed in fig. 5, showing that the detection efficiency is 100% at all zenith angles for $Ne(0) \geq 10^{5.2}$ (corrections (a) and (b) of sect. 2.1 being included). A similar result has been obtained by means of a simulation performed by using the experimental *ldf*.

The obtained shower size spectra for vertical incidence, and for the zenith angles corresponding to the Akeno [2] and MSU [26] atmospheric depths are shown in fig. 6. Also the Akeno and MSU fits are shown for comparison, the Akeno

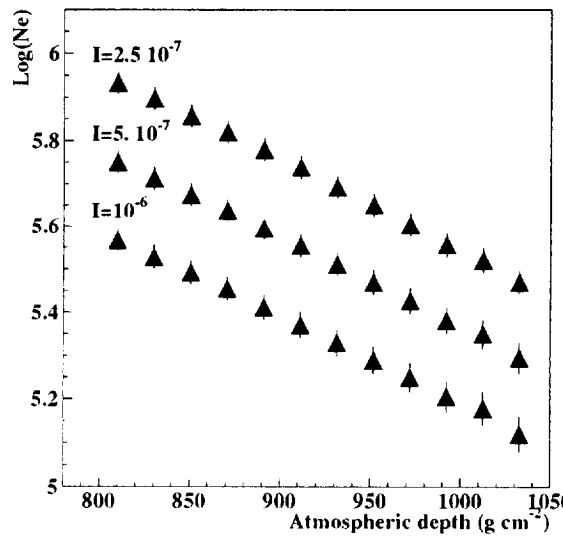

Figure 4. Size values vs. atmospheric depth for different values of primary intensity (see fig. 3).

data being corrected following the transition effect of our array. The data qualitatively agree, the main difference between the present and previous ones consisting in a higher (≈ 30 %) intensity at $N_e \approx 10^{5.2}$, and a slightly steeper slope for large shower sizes (at least with respect to the Akeno data). The break of the spectrum is observed at $Ne \approx 10^6$.

To convert the size spectrum to energy spectrum, the quoted expressions (3) and (4) are used. An effective c.r. primary mass has also to be used:

$$A_{eff}(Ne) = \frac{\sum_i A_i\Phi_i(Ne)}{\sum_i \Phi_i(Ne)} \qquad (7)$$

where $\Phi_i = b_i \cdot E_o^{-\gamma_i}$. b_i and γ_i are obtained from the extrapolations of the direct measurements up to $E_k(A) = Z\ 3 \cdot 10^{15}$ eV, and $\gamma_i \Rightarrow \gamma_i + 0.5$ for $E_o > E_k(A)$ and all nuclear mass groups. The validity of the extrapolation of the lower energy composition data up to the knee is supported by the $Ne - N\mu$ data both for $E_\mu > 1.4$ TeV [27] and $E_\mu > 1$ GeV [28] (see also fig 15). The assumption of the Peters-Zatsepin model at higher energies is compatible with the present

Table 1
Parameters of the differential primary spectra of the different mass groups.

Mass group	b_i $(m^2\ s\ sr\ GeV^{-\gamma})^{-1}$	$\gamma_i(E < E_k(A))$
p	$5.57 \cdot 10^4$	2.86
He	$9.15 \cdot 10^3$	2.68
CNO	$1.18 \cdot 10^3$	2.56
Mg-Si	$1.35 \cdot 10^3$	2.63
Fe	$1.46 \cdot 10^3$	2.63

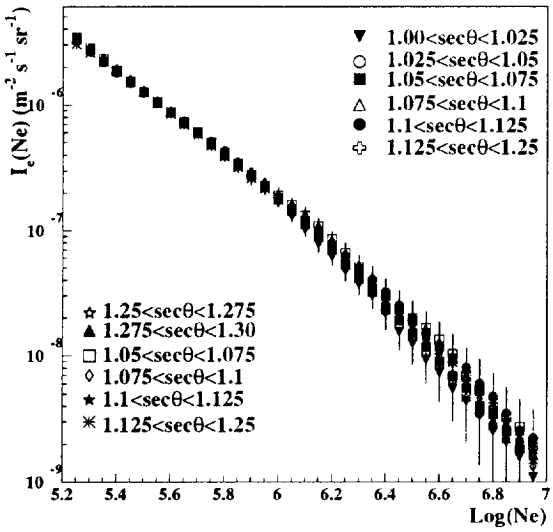

Figure 5. Same as fig. 3, with shower size converted to vertical incidence.

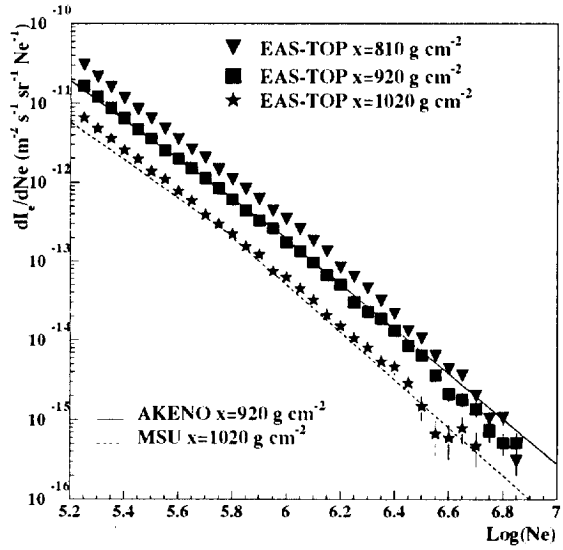

Figure 6. Differential size spectra measured at EAS-TOP at different zenith angles, compared with Akeno and MSU data.

data and mostly supported by the MSU measurements [29,30]. The primary spectra of the different mass groups are reported in tab 1. In the energy range of our interest, around the knee, $A_{eff}(Ne)$ changes from 9 at $Ne = 3. \cdot 10^5$ to 10.5 at $Ne = 10^6$ and 14 at $Ne = 3. \cdot 10^6$.

Assuming constant composition above the knee (i.e. the composition obtained from tab. 1 at $E_o = 3 \cdot 10^{15}$ eV) would imply a change of 10% intensity at 10^{16} eV.

The resulting intensity (shown in fig. 7) below the knee is $\approx$ 20% higher than the MSU and Akeno data, and in good agreement with the recent Tibet ASγ measurements [7], while is $\approx$ 10% lower at $\approx 10^{16}$ eV. The main feature of the present data is given by the shape of the steepening, that looks rather sharp as compared e.g. to the ASγ data (see also sect. 3.2).

Due to such sharpness, for representing the all particle spectrum in the energy range $10^{15} - 10^{16}$ eV, we use the following approximate expression:

$$I(E_o) = I_k \cdot (E_o/E_{o_k})^{-\gamma_{1,2}} \qquad (8)$$

with (1,2)=(below,above) the knee
where:
$I_k = (4.3 \pm 0.8) \times 10^{-23}$ m^{-2} s^{-1} sr^{-1} eV^{-1}
$E_{o_k} = (4.7 \pm 0.3) \times 10^{15} eV$
$\gamma_1 = 2.76 \pm 0.02$
$\gamma_2 = 3.27 \pm 0.08$.

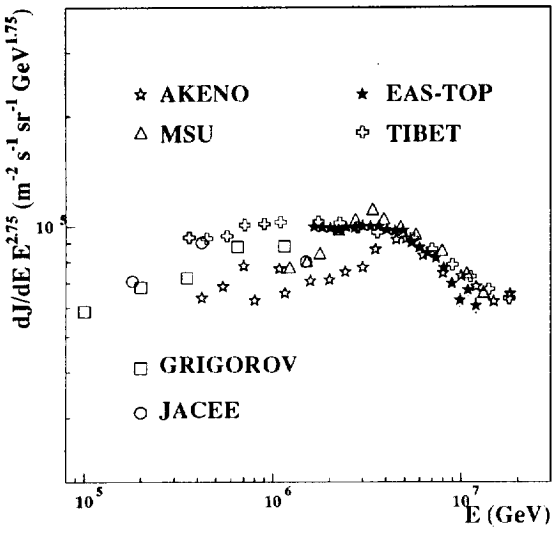

Figure 7. Differential primary energy spectrum measured at EAS-TOP. Direct measurements and EAS data from other experiments are also shown.

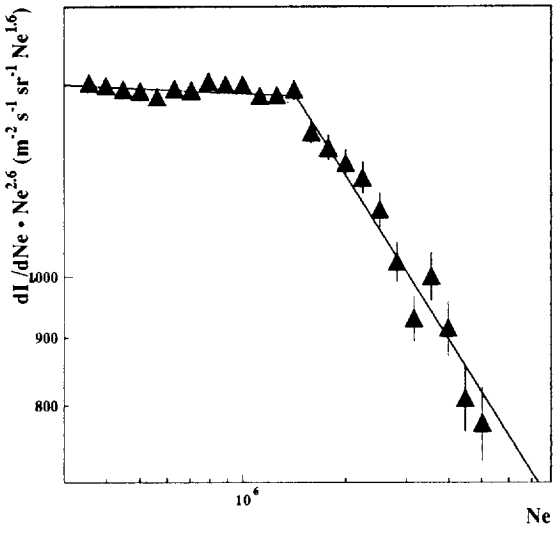

Figure 8. Differential size spectrum, at $x_0 = 810$ g cm^{-2} measured at EAS-TOP.

3.2. The characteristics of the knee in the e.m. component.

In order to evidence the structure of the knee, the size spectrum is shown in fig 8, the ordinate being multiplied by $Ne^{2.6}$. No structure is seen, at a level of $< 10\%$ accuracy in intensity at the break, and 12.5% in size. Even assuming the first point above the break to be dominated by fluctuations, the next point provides evidence for a decreasing of the intensity with respect to the extrapolation of the $Ne < 10^6$ power law index: ($I_{extr.}$-$I_{meas.}$)$\approx$ 4 s.d. (i.e. $\approx$ 8%) for a change $\Delta Ne/Ne \approx 25\%$. Due to the lack of visible structures, the size spectrum around the break is also fitted with an expression (8):

$$I_e(Ne) = I_{e_k} \cdot (Ne/Ne_k)^{-\gamma_{e_1},\gamma_{e_2}} \qquad (9)$$

where:
$I_{e_k} = (1.4 \pm 0.3) \times 10^{-13} m^{-2} s^{-1} sr^{-1} Ne^{-1}$
$Ne_k = (1.41 \pm 0.03) \times 10^6$
$\gamma_{e_1} = 2.61 \pm 0.01$
$\gamma_{e_2} = 3.01 \pm 0.06$
the integral intensity above Ne_k being:
$S_{e_k}(Ne_k) = (9.8 \pm 2.1) \cdot 10^{-8} m^{-2} s^{-1} sr^{-1}$.
It has been argued whether a sharp break could be compatible with a steepening of the primary spectrum, in view of the cascade fluctuations, and the detectors experimental uncertainties. Such effects have been included in a simulation of a break of $\Delta\gamma = -0.5$ over a proton primary spectrum. The reconstructed size spectrum is displayed in fig. 9, and can be directly compared to the experimental one of fig. 8. This shows that a change in the power law index of the energy spectrum of the lighter component, that dominates the shape of the size spectrum, of $\Delta\gamma = -0.5$ would still be compatible with the observed sharpness of the break.

A further controversial problem in establishing the knee has been risen by the difficulties of observing the expected dependence of the size corresponding to the change of the spectral slope (Ne_k) on the observation angle. In fact from observations performed at different atmospheric depths (X_{oss}) a decreasing of Ne_k vs. X_{oss} was qualitatively inferred [31], with large uncertainties mainly due to the difficulties of inter-

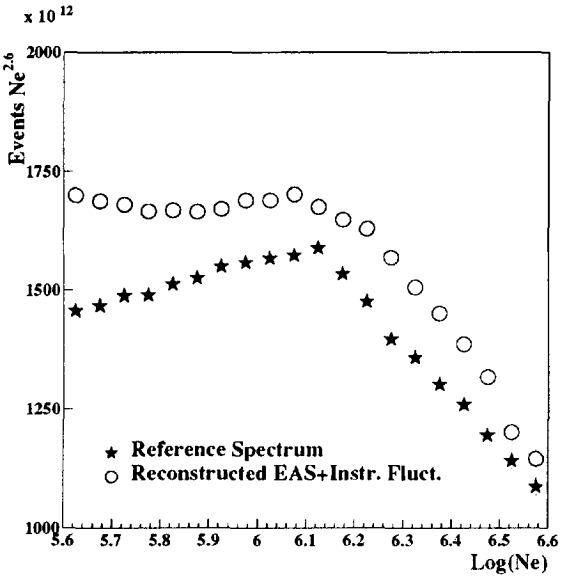

Figure 9. Simulation results: unfluctuated spectrum (i.e. as resulting from the average E_o to Ne conversion) and spectrum obtained including the shower development and the instrumental fluctuations. To be compared to the experimental data of fig. 8.

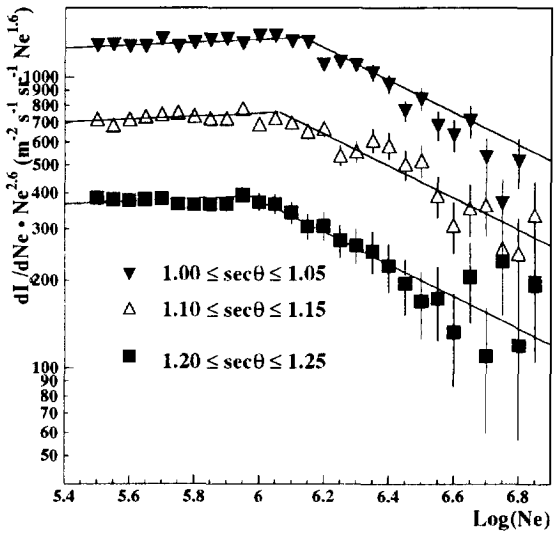

Figure 10. Differential size spectra measured at different zenith angles (i.e. atmospheric depths).

calibrating different detectors. On other side, with angular measurements performed by a single array, such intercalibration problems are overcome, but the observation range is reduced. The present data are shown in fig. 10, where the size spectra measured in different intervals of zenith angles are displayed without including conversion (6). Fits performed by using expression (9) are also shown, and the results are reported in tab. 2: the shift of the value of Ne_k towards lower sizes with increasing zenith angles is clearly visible. The dependance of Ne_k vs X_{oss} is shown in fig. 11. The hypothesis of constancy of Ne_k vs X_{oss} is rejected with a $\chi^2 = 6/\text{d.f.}$, while the hypothesis of the constancy of I_k provides a $\chi^2 = 2/d.f.$.

4. THE MUON DETECTOR DATA

The average muon lateral distribution is shown in fig. 12 for the shower size interval $10^{5.3} < Ne < 10^6$, and $\theta < 17.7°$ ($\sec\theta < 1.05$). The results are compared with the expectations from a simulation based on the Corsika code, and different primaries, including the mixed composition model reported in tab. 1. The very good agreement between the simulated and expected muon lateral distributions (concerning the shape and the absolute values) for the mixed primary composition, allows to use the recorded number of muons to derive the total muon number (muon size, $N\mu$, $E_\mu > 1$ GeV). The used l.d.f. is of Greisen type [32]:

$$\rho_\mu(r) = C(1/r_0)^{1.25}\, N\mu r^{-0.75}(1 + r/r_0)^{-2.5} \quad (10)$$

with $r_o = 400$ m in agreement with the experimental and simulated data.

4.1. The muon size ($N\mu$) spectrum

The muon size distributions obtained for two intervals of core distances ($100 < r < 130$ m and $130 < r < 180$ m) are shown in fig. 13.

Table 2
Size values and differential fluxes at the knee measured in different zenith angle intervals

$\sec\theta$	$I_k(m^{-2}s^{-1}sr^{-1}Ne^{-1})$	$Log(Ne_k)$
1.00 - 1.05	$(1.5 \pm 0.2) \times 10^{-13}$	6.13 ± 0.02
1.05 - 1.10	$(2.0 \pm 0.3) \times 10^{-13}$	6.04 ± 0.02
1.10 - 1.15	$(1.3 \pm 0.2) \times 10^{-13}$	6.06 ± 0.03
1.15 - 1.20	$(1.5 \pm 0.3) \times 10^{-13}$	5.99 ± 0.03
1.20 - 1.25	$(1.2 \pm 0.3) \times 10^{-13}$	5.97 ± 0.04
1.25 - 1.30	$(1.5 \pm 0.4) \times 10^{-13}$	5.87 ± 0.04

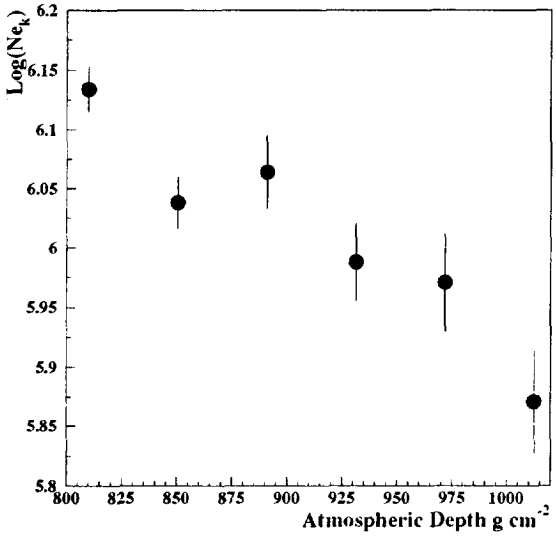

Figure 11. Shower size of the knee as measured at different atmospheric depths.

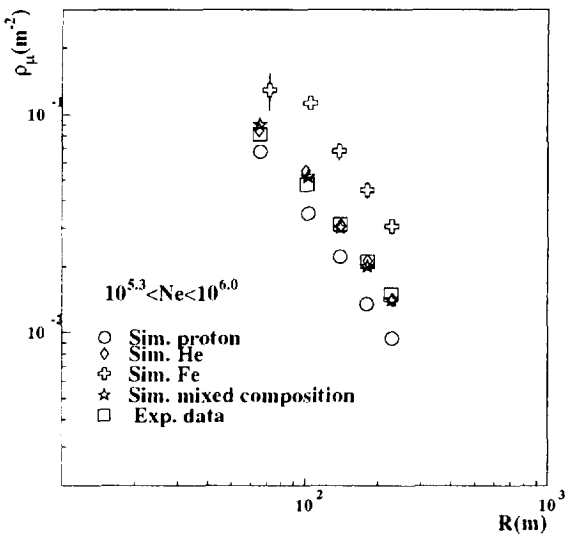

Figure 12. Measured and simulated average muon lateral distributions.

Both of them show a break in the spectrum at $N\mu \approx 10^{4.9}$. This shows that the observed break does not depend on the muon density on the detector, but on the absolute muon number $N\mu$, thus excluding possible effects of instrumental origin. The break is much smoother than observed in Ne, mainly due to the poissonian fluctuations (the typical number of detected muons at the break being $\approx$ 15, for $130 < r < 180$ m). An expression (9) is also used to fit the data at the break:

$$I_\mu(N\mu) = I_{\mu_k} \cdot (N\mu/N\mu_k)^{-\gamma_{\mu_1},\gamma_{\mu_2}} \qquad (11)$$

A χ^2 fit is then performed by introducing the instrumental and poissonian fluctuations, providing as best values of the parameters:
$I_{\mu_k} = (3.5 \pm 0.8) \times 10^{-12} m^{-2}s^{-1}sr^{-1}N\mu^{-1}$
$N\mu_k = (5.89 \pm 0.06) \cdot 10^4$
$\gamma_{\mu_1} = 3.12 \pm 0.03$
$\gamma_{\mu_2} = 3.67 \pm 0.07$
(γ_{μ_2} is in good agreement with data reported by the Akeno array [2]).

The integral intensity above $N\mu_k$ is:
$S_{\mu_k}(> N\mu_k) = (7.7 \pm 1.8)10^{-8} m^{-2}s^{-1}sr^{-1}$
The comparison between the experimental and the simulated spectra (for $130 < R < 180$m) sampled with such parameters, and introducing the

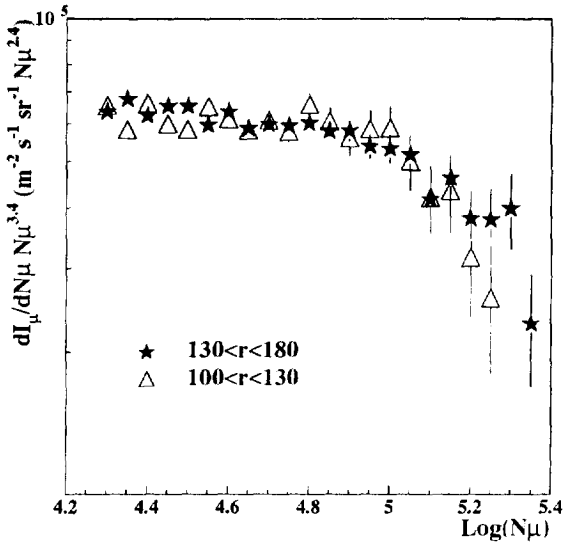

Figure 13. $N\mu$ spectrum measured in two different ranges of core distances.

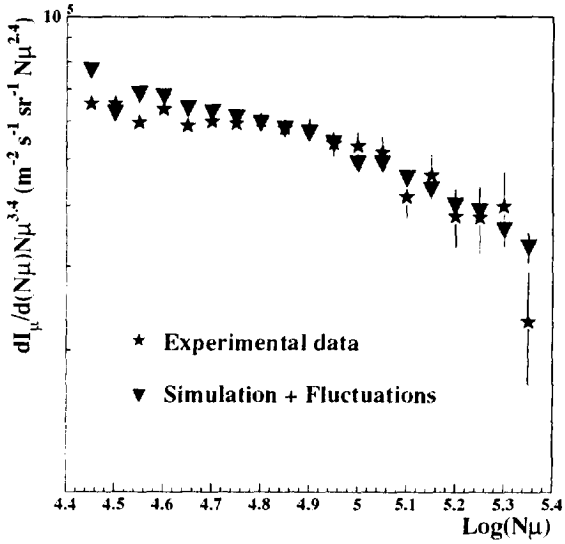

Figure 14. Muon number spectra: experimental and simulated (see text).

poissonian fluctuations is shown in fig. 14.

5. THE E.M. AND MUON DATA

As a first comparison between the e.m. and muon data at the knee we notice the good agreement between the absolute intensities above Ne_k and $N\mu_k$: S_{e_k} and S_{μ_k}, consistent with $\approx 10^{-7} m^{-2} s^{-1} sr^{-1}$.

In fig. 15 the experimental relation $N\mu - Ne$, and the expectations from the Corsika code and different primaries, including the mixed primary composition of tab.1, are shown. The experimental data cover all the range, while the simulated ones cover the region below the knee, and a single size bin $4. \cdot 10^6 < Ne < 5. \cdot 10^6$ above the knee. The data are well superimposed over the expectations from the mixed composition of tab. 1. Also shown are the expectations from a mixed composition with the knee occurring at fixed primary energy ($3. \cdot 10^{15}$ eV) for all components. In the bin above the knee the slightly heavier composition, as predicted by the Peters-Zatsepin hypothesis seems favoured (although due to the statistics and the model dependence we do not discuss the primary composition problem at this stage of the analysis).

Also shown in fig.15 is the error box around the Ne_k and $N\mu_k$ values. 3 s.d. boundaries are used in order to take into account systematic effects connected with the binning and the selection procedure. It results that the $Ne_k - N\mu_k$ data cross very well over the $Ne - N\mu$ experimental relation, thus showing that they identify the same primary energy.

Further information is obtained from the relation between the γ_{e_1} and γ_{μ_1} (and γ_{e_2} and γ_{μ_2}) values, i.e. the slopes of the spectra, below and above the break. They are shown in fig. 16 together with the expectations from the general relation $N\mu \approx Ne^{\alpha}$ and different values of α. A value of $\alpha \approx 0.75$ is compatible with the experimental data both below and above the break.

The main features of the breaks of the Ne and $N\mu$ spectra are thus compatible in intensity, identification of the primary energy and change of slope inside experimental uncertainties $\approx 15\%$.

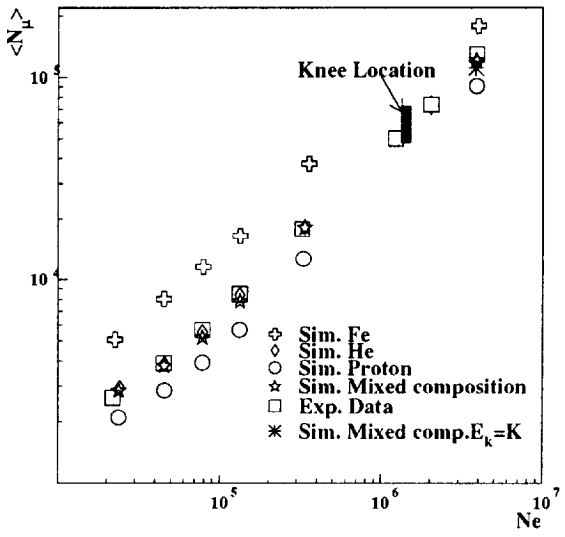

Figure 15. Mean values of $N\mu$ in different Ne intervals (data and simulation).

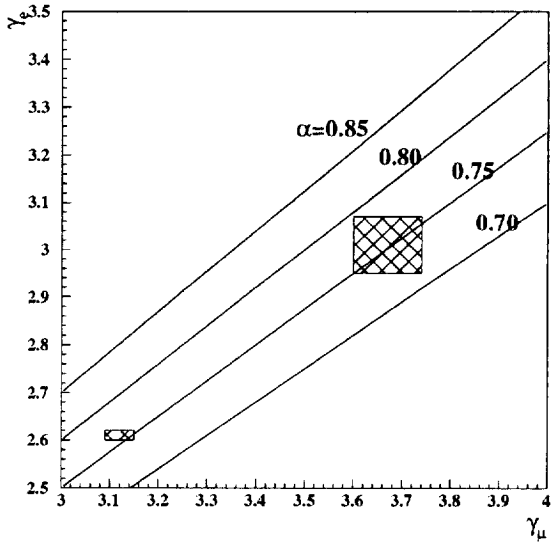

Figure 16. Relation between the exponents of the electrons and muons power law size spectra (γ_e, γ_μ) below and above the knee.

6. THE ANISOTROPY

The study of the anisotropy and its possible variations is, as mentioned, a fundamental tool for discriminating possible astrophysical origins of the knee. In this field also, it is of first interest to check the validity of the methods used for the interpretation of the information on c.r. propagation at high energies.

The c.r. anisotropy is studied with good statistical significance in the energy range $10^{11} - 10^{14}$ eV ([33–40], see the reviews [41,42]).

A few of such data are summarized in fig. 17. At the highest energies (above 10^{14} eV) significant results have been recently reported by the EAS-TOP array [39,40]. The amplitude and phase of the first harmonic of the sidereal anisotropy are respectively (at the equatorial plane):

$A_{sid} = (3.73 \pm 0.57) \cdot 10^{-4}$

$\phi_{sid} = 1.82 \pm 0.49$ h lst

with significance 6.5 s.d.

This result is supported by different consistency checks:

a) the observation of the solar anisotropy:

$A_{sol} = (4.06 \pm 0.55) \cdot 10^{-4}$

$\phi_{sol} = 4.92 \pm 0.53$ h

with significance 7.3 s.d.,

compatible, within 2 s.d., with the Compton-Getting effect due to the revolution of the Earth around the Sun:

$A_{sol}^{CG} = 4.7 \cdot 10^{-4}$

$\phi_{sol}^{CG} = 6.0$ h;

b) the observation of the expected dependence of the amplitude of the anisotropy over the declination (δ):

$A \propto cos(\delta)$;

c) the consistent time shifts of the effect for observations in the East and West directions;

d) the small antisidereal wave (of amplitude $A < 2.2$ s.d.);

e) the correct rotation of the monthly solar vector, as resulting from the combination of the solar and sidereal vectors.

Different experiments [29,30], mostly based on the $Ne - N\mu$ relation and muon fluctuation data, support an increase of the average mass number

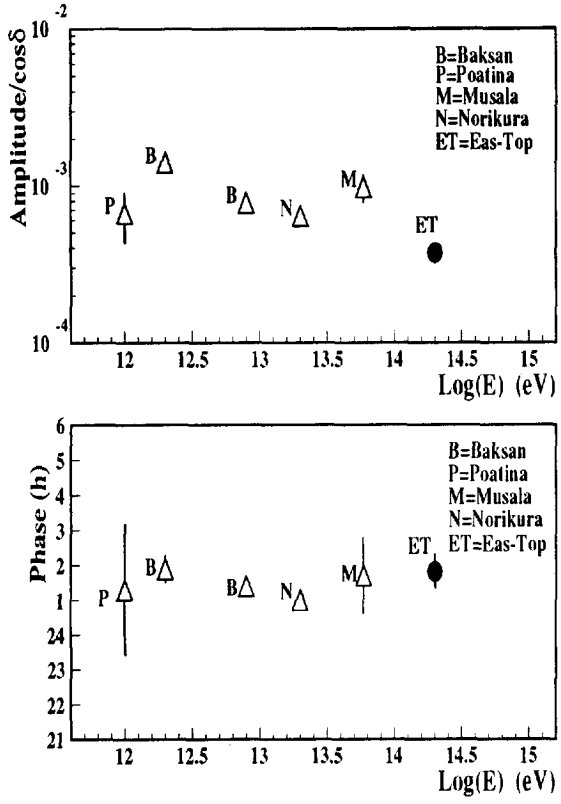

Figure 17. Amplitudes and phases (h, l.s.t.) of the c.r. anisotropy reported in the energy range $10^{12} - 10^{14}$ eV, including the EAS-TOP data.

of the primaries around the "knee", as would be expected from the diffusion hypothesis [10,11]. A diffusion model has been developed at lower energies to explain the $\bar{p}$ flux, the e^+ to e^- and the secondary to primary ratios and their energy dependence (see e.g. [43,44]). The general parameters of the model (diffusion coefficient $D(R) \approx 10^{28} \cdot R^{0.3}$ cm^2 s^{-1}, R in GV) can be extrapolated and used to predict the anisotropy at $E_o > 10^{12}$ eV.

It results that, while the amplitude of the anisotropy measured at 10^{12} eV could be compatible with the expectations, the experimental data around 10^{14} eV are lower than the expectations (in the case of EAS-TOP of a factor ≈ 10). This implies that the diffusion model as constructed at $10^9 - 10^{11}$ eV cannot be extrapolated to 10^{14} eV (see e.g. [45,46]).

On the other side it is confirmed that the amplitude and the phase of the anisotropy are rather constant over the whole quoted energy range $10^{12} - 10^{14}$ eV.

7. CONCLUSIONS

The first studies of the "knee" region of the cosmic ray primary spectrum from the EAS-TOP array lead to the following results:

- The break at $E_o = (3-5) \cdot 10^{15}$ eV is confirmed both from the electron and muon EAS components.
- The data from Ne and $N\mu$ agree both concerning the primary energy and intensity at the knee ($I_k \approx 10^{-7}$ cm^{-2}s^{-1}sr^{-1}), and the variations of the spectral indexes.
- The γ_e, γ_μ data below and above the knee do not show indications of change of the $Ne \approx N\mu^\alpha$ relation (α is constant within $\approx 5\%$).
- The knee is sharp, but compatible with a change in the spectral index (of $\Delta\gamma \approx -0.5$) of a single component, the lighter one, dominating the shape of the size spectrum.
- The steepening in Ne is observed at decreasing shower size with increasing zenith angles (observation level in the atmosphere).
- The $Ne - N\mu$ relation (both for GeV and TeV muons) does not evidence dramatic changes in primary composition around the knee. For more quantitative analysis in terms of primary composition, the combined study of different EAS components is being exploited.
- Different experiments (also compatibile with the present data) report a primary composition becoming heavier above the knee, as predicted by the diffusion models. But the anisotropy data contradict the naive extrapolation of the diffusion model

derived from the low energy measurements, and no evidence can be derived up to $\approx 2. \cdot 10^{14}$ eV of any increase of the amplitude of the anisotropy itself, as it would be expected from models based on such propagation principles.

REFERENCES

1. G.V. Kulikov and G.B. Khristiansen, JEPT, 35 (1958) 35
2. M. Nagano et al., J. Phys. G, 10 (1984) 1295
3. D.S. Adamov et al., Proc. 21th I.C.R.C., 9 (1990) 260
4. T.V. Danilova et al., J. Phys. G, 19 (1993) 429
5. The EAS-TOP Collaboration, Proc. 24th I.C.R.C., 2 (1995) 732
6. I.N. Kirov et al., Proc. 17th I.C.R.C., 2 (1981) 109
7. M. Amenomori et al., Ap. J., 461 (1996) 408
8. S.V. Bryanski et al, Proc. 24th I.C.R.C., 2 (1995) 724
9. A.E. Chudakov et al, Proc. 18th I.C.R.C., 6 (1983) 29
10. B. Peters, Proc. 6th I.C.R.C., 3 (1959) 157
11. G.T. Zatsepin et al, Izv. Akad. Nauk USSR S.P., 26 (1962) 685
12. C. Cesarsky and P. Lagage, Proc. 17th I.C.R.C., 9 (1981) 250
13. A.M. Hillas, Proc. 16th I.C.R.C., 8 (1979) 7
14. P.L. Bierman, Proc. 23rd I.C.R.C., Invited, Rapporteur and Highlight Papers (1994) 45
15. S.I. Nikolsky, Nuclear Physics B, 39A (1995) 228
16. B.A. Khrenov, Nuclear Physics B, 33A (1993) 18, and references therein
17. A.D. Erlykin, Nuclear Physics B, 39A (1995) 215, and references therein
18. M. Aglietta et al, Il Nuovo Cimento, 9C (1986) 262
19. M. Aglietta et al, Nuclear Instr. Meth. in Phys. Res., A277 (1989) 23
20. M. Aglietta et al, Nuclear Instr. Meth. in Phys. Res., A336 (1993) 310
21. K. Kamata et al., Suppl. Prog. Theor. Phys., 6 (1958) 93
22. K. Greisen, Progr. in Cosmic Ray Phys., 3 (1956)
23. R. Brun et al., GEANT3 User's Guide, CERN DD/EE/84-1, 1984
24. J.N. Capdevielle et al, KfK Report 4998 (Karlsruhe, 1992)
25. EAS-TOP Coll., Proc. 23rd I.C.R.C., 4 (Calgary, 1993) 251
26. Yu. A. Fomin et al, Proc. 22th I.C.R.C., 2 (1991) 85
27. M. Aglietta et al (MACRO and EAS-TOP colls.), Physics Letters B, 35 (1994) 376, Proc. 24th I.C.R.C., 2 (1995) 710
28. EAS-TOP Coll., Proc. 24rd I.C.R.C., 2 (Roma, 1995) 664, Il Nuovo Cimento, in press
29. G.B. Khristiansen et al., Astrop. Phys., 2 (1994) 127
30. K. Mitsui et al, Astrop. Phys., 3 (1995) 125
31. A.M. Hillas, Phys. Rep., 20C (1975) 59
32. K. Greisen, Ann. Rev. Nucl. Sci., 10 (1960) 63
33. T. Gombosi et al, Proc. 15th I.C.R.C., 11 (1977) 109
34. H. Ueno et al, Proc. 19th I.C.R.C., 5 (1985) 35
35. J.E. Humble et al, Proc. 19th I.C.R.C., 5 (1985) 39
36. Yu. M. Andreyev et al, Proc. 20th I.C.R.C., 2 (1987) 22
37. V.V. Alekseenko et al., Proc. 17th I.C.R.C., 2 (1981) 146
38. K. Nagashima and S. Mori, Proc. Int. Simp. on H.E Cosmic Ray Modulation, Tokyo (1976) 326
39. The EAS-TOP Collaboration, Proc. 24th I.C.R.C., 2 (1995) 800
40. The EAS-TOP Collaboration, Ap. J., in press
41. P. Kiraly et al, Rivista del Nuovo Cimento, 2 (1979) 7
42. J. Linsley, Proc. 18th I.C.R.C., Rapp. Paper (1983) 165
43. V. Ptuskin, 24th I.C.R.C., Rapp. papers (1995) in press
44. T. Shibata, 24th I.C.R.C., Rapp. papers (1995) in press
45. W.I. Axford et al., Proc. 21st I.C.R.C., 3 (Adelaide, 1990) 311
46. V.S. Berezinsky, Proc. 21st I.C.R.C., 11 (Adelaide 1990) 115